Zeolites

International Edition: DOI: 10.1002/anie.201809343
German Edition: DOI: 10.1002/ange.201809343

Achieving Atomic Dispersion of Highly Loaded Transition Metals in Small-Pore Zeolite SSZ-13: High-Capacity and High-Efficiency Low-Temperature CO and Passive NO_x Adsorbers

*Konstantin Khivantsev, Nicholas R. Jaegers, Libor Kovarik, Jonathan C. Hanson, Franklin (Feng) Tao, Yu Tang, Xiaoyan Zhang, Iskra Z. Koleva, Hristiyan A. Aleksandrov, Georgi N. Vayssilov, Yong Wang, Feng Gao, and János Szanyi**

Abstract: *The majority of harmful atmospheric CO and NO_x emissions are from vehicle exhausts. Although there has been success addressing NO_x emissions at temperatures above 250 °C with selective catalytic reduction technology, emissions during vehicle cold start (when the temperature is below 150 °C), are a major challenge. Herein, we show we can completely eliminate both CO and NO_x emissions simultaneously under realistic exhaust flow, using a highly loaded (2 wt %) atomically dispersed palladium in the extra-framework positions of the small-pore chabazite material as a CO and passive NO_x adsorber. Until now, atomically dispersed highly loaded (> 0.3 wt %) transition-metal/SSZ-13 materials have not been known. We devised a general, simple, and scalable route to prepare such materials for Pt^{II} and Pd^{II}. Through spectroscopy and materials testing we show that both CO and NO_x can be simultaneously completely abated with 100 % efficiency by the formation of mixed carbonyl-nitrosyl palladium complex in chabazite micropore.*

Metals loaded into zeolites have become enormously important in recent years due to the ability of their pores to confine metal species.[1–16] Small-pore zeolites also exhibit enhanced hydrothermal stability in comparison to their medium- and large-pore analogues.[17] For example, SSZ-13 (a zeolite with CHA structure), first synthesized by Zones et al., at Chevron,[18] attracted a lot of attention because of its high hydrothermal stability.[19] Cu-SSZ-13 has been commercialized for NH_3 selective catalytic reduction (SCR) of NO_x by BASF. Under the low-temperature SCR conditions the Cu sites (initially atomically dispersed) were suggested to form dynamic Cu-O-O-Cu pairs as the rate-limiting step of O_2 activation.[20,21] However, at copper loading levels relevant to SCR (and methane oxidation) from 1 to 4 wt %, various forms of copper (including CuO_x clusters) coexist even in zeolites (SSZ-13 and MOR).[22,23] The introduction of transition-metal cations of large ionic radii into small pore zeolites using traditional post-synthetic preparation methods (e.g., ion exchange) has proven difficult. Therefore, new methods in which metal precursors are introduced into the zeolite synthesis gel prior to zeolite crystal nucleation have been proposed.[24,25] Today, there is a great interest to produce small-pore zeolites loaded with atomically dispersed Pt and Pd at levels higher than 0.3 wt %. However, methods of loading transition metals ionically into SSZ-13 at practically relevant levels (> 1 wt %) are not known.[16,26–34] Molliner et al. demonstrated a route to produce 0.23 wt % atomically dispersed Pt in SSZ-13 with Si/Al ratio 7 to 9.[16] To form ionically dispersed Pt in SSZ-13, a Pt^{2+} complex with (3-mercaptopropyl)trimethoxysilane ligand had to be added to the zeolite synthesis gel prior to crystallization. On the basis of EXAFS and HAADF-STEM data, it was concluded that Pt was atomically dispersed after calcination of the as-prepared materials in oxygen. Unfortunately, no FTIR (the most sensitive technique to estimate the metal dispersion) data of adsorbed CO was provided to understand speciation of Pt species.[11,26] EXAFS is not sensitive to the minority phases (< 10 %) and HAADF-STEM imaging is a local technique. In prior studies on Pt- and Pd-loaded (0.4–1 wt %) ZSM-5, the IR spectra of room temperature adsorbed CO *always* indicated the presence of Pt and Pd nanoparticles as a consequence of metal agglomeration.[27–31]

Our interest to synthesize Pd/SSZ-13 materials is spurned by their potential application as passive NO_x adsorbers (PNA). PNA is a novel concept proposed to alleviate the problem of NO_x abatement at low temperatures (< 150 °C). Most NO_x emissions from internal combustion engines occur during cold-start when the SCR catalyst is still inactive.[35–46] This is the major source of NO_x pollution in the world and it affects public health and atmospheric chemistry. We have shown that Pd-loaded zeolites were able to store NO_x at low

[*] K. Khivantsev, N. R. Jaegers, L. Kovarik, Y. Wang, F. Gao, J. Szanyi
Institute for Integrated Catalysis
Pacific Northwest National Laboratory
Richland, WA 99352 (USA)
E-mail: janos.szanyi@pnnl.gov

N. R. Jaegers, Y. Wang
Voiland School of Chemical Engineering and Bioengineering, Washington State University
Pullman, WA 99163 (USA)

J. C. Hanson
Chemistry Department, Brookhaven National Laboratory
Uptown, NY 11973 (USA)

F. Tao, Y. Tang, X. Zhang
Department of Chemical and Petroleum Engineering and Center for Environmentally Beneficial Catalysis, University of Kansas, Lawrence, KS, 66045 (USA)

I. Z. Koleva, H. A. Aleksandrov, G. N. Vayssilov
Faculty of Chemistry and Pharmacy, University of Sofia
1126 Sofia (Bulgaria)

Supporting information and the ORCID identification number(s) for the author(s) of this article can be found under: https://doi.org/10.1002/anie.201809343.

temperatures as NO^+ and $Pd^{I/II}$-NO nitrosyl complexes. However, in the engine exhaust gas mixture H_2O is always present in significant amounts: H_2O competes for Pd sites and blocks NO adsorption.[46] The active site in such systems are Pd ions. In order to optimize PNA performance, the concentration of ionically dispersed Pd in the zeolite micropore has to be maximized. In our initial study we used H-forms of zeolites (SSZ-13, ZSM-5 and Beta) with the same Si/Al ratio of 12 to load Pd by the incipient wetness impregnation (IWI) method. The PNA performance of the thus prepared Pd/zeolite materials was satisfactory and comparable to the best state-of-the-art literature but the Pd was underutilized, that is, NO/Pd $\ll$ 1 (Figure S1, see Supporting Information Methods on page 3 for experimental setup and conditions). The discussion regarding why H-forms of zeolite are not effective at producing higher loading of atomically dispersed species[29,34] and how we found the right method[47–50] (we call this method "modified ion exchange") to make such materials is provided in the Supporting Information "Methods" section (pages 1–2).

We used "modified ion-exchange" to prepare 1 wt% loading of Pd on NH_4-SSZ-13 with Si/Al ratios 6, 12, and 30. We chose SSZ-13 because it has the highest hydrothermal stability among all zeolites and it shows ideal temperature for NO_x release $>$ 300 °C (Figure S1 in the Supporting Information). After loading the metal precursor onto NH_4-SSZ-13 the materials were calcined at 650 °C in air. The PNA performance of these three materials with different Si/Al ratios is displayed in Figure S2. HAADF-STEM images (Figure 1, Figures S3–5) of the calcined Pd/SSZ-13 materials show an important trend: complete absence of nanoparticles at Si/Al = 6, the appearance of small 1–2 nm PdO nanoparticles at Si/Al = 12 and the presence of large PdO particles at Si/Al = 30.

The measured NO/Pd = 1 for the 1 wt% Pd/SSZ-13 sample with Si/Al = 6 (Figure S2) further corroborates the 100% dispersion of Pd. For Si/Al 12 and 30, correspondingly, the NO/Pd ratios were 0.87 and 0.3, indicating progressive agglomeration of Pd as the Si/Al ratio increases (XRD data for these materials are shown in Figure S17).

In addition to HAADF-STEM imaging and PNA performance testing, we further characterized the 1 wt% Pd/SSZ-13 (Si/Al = 6) sample with EXAFS and FTIR spectroscopies. XANES region of the EXAFS spectrum (Figure 2) from this material revealed that the Pd ions were present in the +2 oxidation state. Analysis of the full EXAFS spectrum substantiated the absence of both Pd-O-Pd and Pd-Pd bonds and the Pd site can be approximated as $Pd_1O_{(3-4)}$.

Since Pd^{2+} is a d^8 ion, that prefers square planar environment, we assign the sites present in the 1 wt% Pd/SSZ-13 material to Pd_1O_4. DFT calculations (Table S1, Figure S8) further corroborate this point, and the DFT calculated average Pd–O bond (2.09 Å) is in good agreement with $Pd^{II}{}_1O_4$ site suggested by the EXAFS data (2.03 Å). Pd^I and

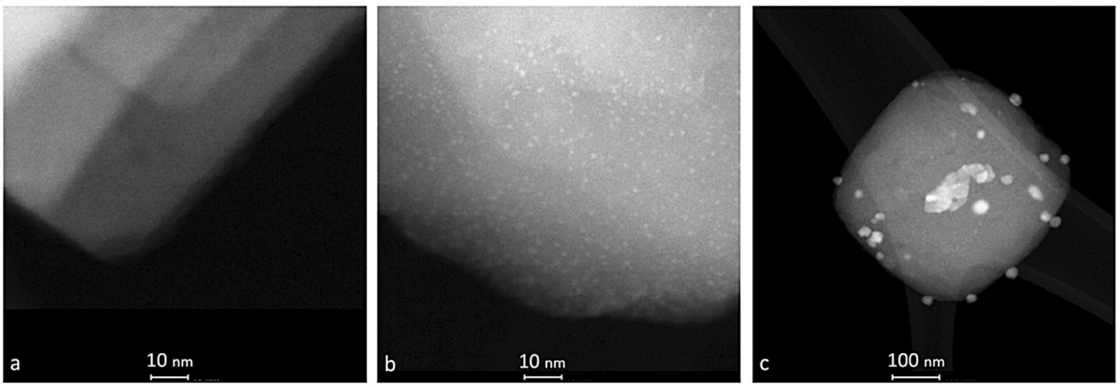

Figure 1. HAADF-STEM images of 1 wt% Pd/H-SSZ-13 a) Si/Al = 6, b) Si/Al = 12, c) Si/Al = 30.

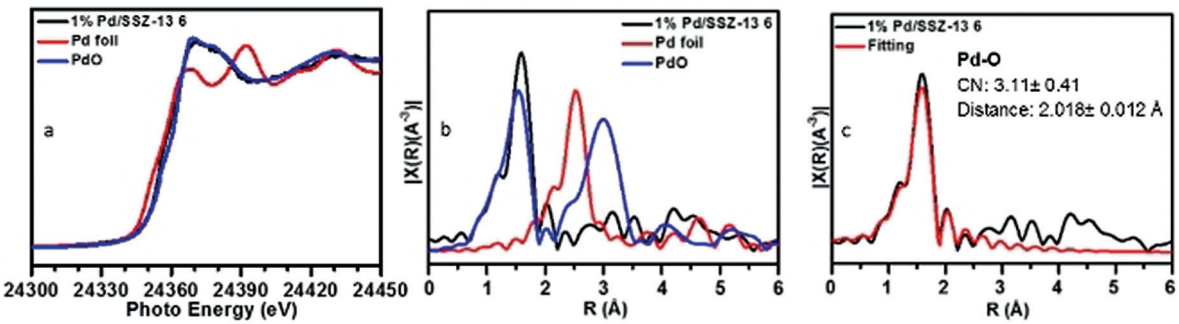

Figure 2. a) XANES region of the 1 wt% Pd/SSZ-13 Si/Al = 6 and references Pd foil and PdO, b) Fourier transform of k^2-weighted EXAFS spectra in the R-space for 1 wt% Pd/SSZ-13 Si/Al = 6, Pd foil and PdO, c) Coordination number and bond lengths of Pd-O in 1 wt% Pd/SSZ-13 Si/Al = 6 and the corresponding fit.

Pd^{III} have significantly longer Pd–O bonds, thus, their presence in the calcined sample cannot be substantiated; however, they may be present in quantities below the detection limit of the EXAFS technique.

The state of Pd in 1 wt% Pd/SSZ-13 (Si/Al = 6) was further investigated by FTIR spectroscopy with NO and CO probe molecules (Figure 3).[11,26,28–31,50] The assignment of the IR bands to specific adsorbed species was supported by DFT calculations. NO- and CO containing metal complexes have high molar extinction coefficients, and thus can provide a detailed picture on the speciation of $M^{n+/0}$ species. NO adsorption on 1 wt% Pd^{II}/SSZ-13 with Si/Al = 6, leads to the appearance of three absorption bands in the NO stretching region (Figure 3a): a broad band (FWHM ≈ 80 cm^{-1}) centered at 2170 cm^{-1}, and two narrower (FWHM ≈ 25 cm^{-1}) features at 1860 and 1805 cm^{-1}. Note that no peaks can be assigned to NO adsorbed on reduced Pd clusters/nanoparticles. The 2170 cm^{-1} feature represents the $\nu_{N\text{-}O}$ vibration of NO^+ species located in the extraframework positions of the zeolite.[51,52] DFT calculations presented in the Supporting Information (Table S1) confirm assignments of the 1865 cm^{-1} feature to a Pd^{2+}-NO complex and the 1805 cm^{-1} band to Pd^+-NO.

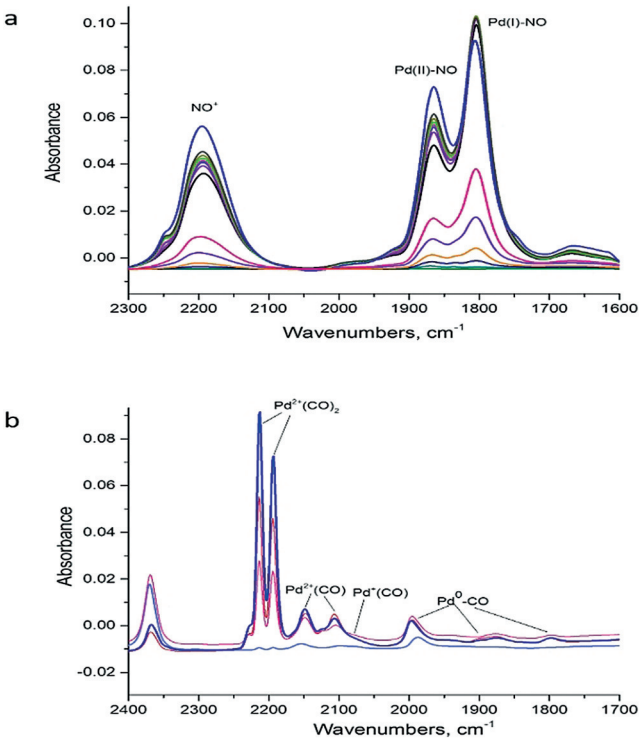

Figure 3. Series of FTIR spectra recorded during a) NO adsorption (2 torr, 20 °C) and b) CO adsorption (5 torr, 20 °C) on 1 wt% Pd/H-SSZ-13 (Si/Al = 6).

In the absence of oxygen NO^+ is formed by a direct electron transfer from the NO radical to Pd^{2+} (analogous to the previously described mode of Cu^{2+} reduction in SSZ-13 by NO with the formation of a Cu^+-NO complex). This electron transfer reduces Pd^{2+} to Pd^+, releasing the vacant cationic site onto which the nitrosyl ion NO^+ anchors. CO adsorption (Figure 3b) leads to the predominant formation of $Pd^{n+}(CO)_2$ species (with CO frequencies 2214–2193 cm^{-1}, we tentatively assign $n = 2$), $Pd^{2+}(CO)(OH)$ and $Pd^{2+}(CO)$ species (with CO frequencies ca. 2150–2115 cm^{-1}), $Pd^+(CO)$ (with CO frequencies ca. 2075 cm^{-1}) and small Pd clusters $Pd_x(CO)_y$ with CO linear stretch at around 2000 cm^{-1} and some bridged CO < 1950 cm^{-1} produced in small amounts (total fraction < 3% of total observable Pd). This is the highest dispersion of 1 wt% Pd/Zeolite material that has ever been observed by FTIR of adsorbed CO at ambient temperature. DFT calculations allowed us to assign and exclude the possible formation of Pd-O-Pd dimeric sites in SSZ-13 (Table S1, Figure S8). Thus, we conclude that Pd is ionically dispersed in the SSZ-13 framework.

The 1 wt% Pd-SSZ-13 (Si/Al = 6) material synthesized by this new method has an NO/Pd = 1 storage efficiency that translates to a storage capacity of 94 micromole g^{-1}. Compared to the state-of-the-art materials described in the open and patent literature (see Table S2 for comparison), this material exhibits approximately 50% higher NO storage capacity under industrially relevant conditions than its best reported contender 1 wt% Pd/BEA and 2 times higher than the best reported 1 wt% Pd/SSZ-13 (Table S2). This result brings up the question whether we can further increase the amount of NO_x stored in the Pd-loaded zeolite materials by simply increasing the metal loading. To this end we prepared additional Pd-SSZ-13 storage materials with metal loadings of 1.9, 3, and 5 wt%. We can assume that PNA performance, expressed as NO/Pd ratio, is directly proportional to Pd dispersion since PdO particles do not store NO_x. In fact, we found that for 1.9 wt% Pd/SSZ-13 (Si/Al = 6) the NO/Pd = 1 still holds (Figure 4).

Additional increase in Pd loading to 3 wt%, however, resulted in deviation from this value, as the NO/Pd ratio dropped to 0.9, still a rather high storage efficiency, indicating

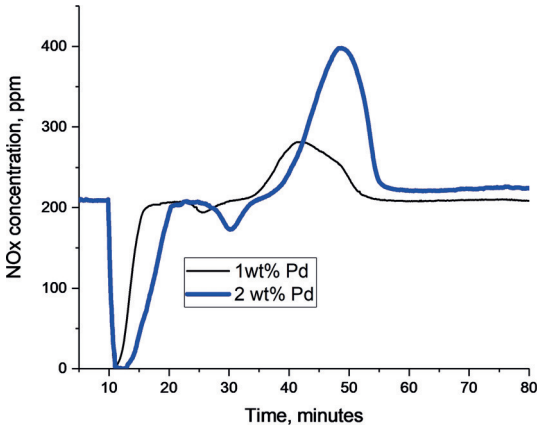

Figure 4. PNA performance of 1 and 1.9 wt (marked as 2 wt%) Pd SSZ-13 with Si/Al = 6. NO_x adsorption at 100 °C for 10 min (after 10 min bypass) followed with TPD (10 °C min^{-1}). The feed gas mixture contains 200 ppm of NO_x, 14% O_2, 3% H_2O with 200 ppm CO. Note that for 1.9 wt% Pd/SSZ-13 more time was needed for the NO_x to return to the initial level owing its high effectiveness at abating NO_x; desorption of NO_x, therefore, was started after approximately 23 minutes.

90% of Pd is dispersed atomically. Increasing the metal loading to 5 wt% resulted in the decrease in NO/Pd ratio to 0.7 (Figure S6). Full utilization of Pd is achieved for materials with Pd loading up to 2 wt%, and the amount of NO stored was 94, 180, 250 μmole g^{-1} for 1, 1.9, and 3 wt% samples, respectively. Some agglomeration of PdO on the 5 wt% Pd loaded SSZ-13 (Si/Al = 6) material ultimately led to a decreased NO_x storage efficiency (Figure S6).

The most important consequence of these unprecedented NO_x storage capacities is the complete NO_x removal from the exhaust gas stream for an extended period of time (ca. up to 100 s for 2 wt% Pd). Stored NO_x is released during temperature ramp between 250 and 450 °C.

FTIR confirms selective transformation of Pd^{II}-NO species to a mixed carbonyl-nitrosyl complex $Pd^{II}(NO)(CO)$ in the presence of CO (Figure S7). The stability of this complex, all its bond lengths and the assignment of its frequencies was fully corroborated by DFT (Figure S8, Table S1). Despite the fact that DFT predicts $Pd(CO)(NO)_2$ complex to be more stable, the NO/Pd ratio and FTIR reveal that only $Pd^{II}(NO)(CO)$ can be formed under conditions relevant to PNA. DFT calculations further confirm the formation of the bent M-N-O bond[53,54] which explains why Pd/Zeolite system is able to store NO efficiently: bent M-N-O corresponds to a covalent bond, much stronger than, for example, linear M-C-O fragments in metal carbonyl complexes. This highlights the importance of using experimental and computational approaches together in order to correctly identify characteristics of adsorbed species. Owing to the formation of $Pd^{II}(NO)(CO)$ complex, CO is adsorbed on the Pd site analogous with NO. This allows unprecedented complete removal of CO from exhaust stream at 100 °C during cold start together with NO (Figure S9).

This result further confirms the stoichiometry of the $Pd^{II}(NO)(CO)$ complex derived directly from the PNA performance measurement under simulated lean exhaust feed. The next question we sought to answer was: why does the dispersion of Pd decrease as the Si/Al ratio increases at a specific Pd loading? Pd loaded SSZ-13 samples with Si/Al ratios of 12 and 30 exhibited the formation of progressively larger PdO_x nanoparticles and not all Pd was dispersed (unlike in the sample with Si/Al = 6). This happened despite the abundance of Brönsted acid sites in the zeolite structure: for example, for 1 wt% Pd/SSZ-13 with Si/Al ratio 30 the nominal $[H^+]/Pd^{II}$ ratio is approximately 6. The answer is most certainly related to the increased hydrophobicity of the zeolite with increasing Si/Al ratio. Owing to increasing hydrophobicity inside the zeolite channels at lower Al content, the aqueous solution containing the Pd precursor cannot infiltrate the pores. Water transport through the micropores in the confined (< 1 nm) space of SSZ-13 has a barrier. We performed water TPD on H-SSZ-13 materials with Si/Al of 6, 12, and 30 (Figure S10): the amount of water adsorbed in the micropores decreased dramatically as the Si/Al ratio increased from 6 to 30, as well as the strength of zeolite interaction with water as evidenced by the shift of the TPD peak to higher temperatures with a decrease in Si/Al ratio. Thus, we highlight hydrophilicity of the zeolite as another important factor affecting the aqueous preparation of metal-loaded small/medium pore zeolites. This explains the discrepancies in the literature regarding the preparation of different transition metal loaded small and medium-pore zeolites.[27–32] In those papers, the materials are prepared via either reaction with H-form of the zeolite (which is not effective) or using materials with high Si/Al ratios (10 and higher). Owing to the less hydrophilic nature of these materials, not all of the precursor in aqueous solution can access the sites inside the zeolite pores. For such materials, aqueous preparation route will not produce highly loaded atomically dispersed metal species, and other more complex and expensive methods are required, such as use of chemical vapor deposition of a volatile organometallic precursor or loading an organometallic precursor in a non-polar solvent.[11,53]

This also indicates that there is no diffusion limitation for Pd and Pt to enter the micropores of SSZ-13, as was previously suggested.[16,34] The Si/Al ratio of these siliceous materials should be ($3 < x < 10$) sufficient to utilize all metal and produce enough metal in the micropore.

Will the preparation method proposed here for Pd/SSZ-13 work with other transitions metals? To this end we prepared Pt/SSZ-13 using the same procedure. With current methods Pt loadings (with atomic Pt dispersion) of only < 0.3 wt% can be achieved in SSZ-13 (with Si/Al ratios between 7 and 8).[34] In contrast, with the utilization of our new method, we were able to load 1 wt% atomically dispersed Pt in SSZ-13. FTIR with CO confirmed complete ionic dispersion of Pt: no CO peaks attributable to metallic Pt appeared (Figure S11) and only peaks from CO on ionic platinum Pt^{II} > 2119 cm^{-1} were present.[11] The data are nicely corroborated by HAADF-STEM images (Figure 5).

No Pt clusters are observed (only when the zeolite begins to amorphize owing to inevitable beam damage under the electron beam, does the appearance of small bright features that are small Pt clusters becomes evident; see additional images in Supporting Information, Figures S12–S14).

We also discovered that Pt/SSZ-13 synthesis (unlike for Pd/SSZ-13) is sensitive to calcination conditions. When the 1 wt% Pt/SSZ-13 (Si/Al = 6) sample was calcined at 350 °C in air, no Pt agglomeration was observed. Calcination at 400 °C, however, resulted in the formation of metallic Pt nanoparticles on the external surface of the zeolite crystals (Figure S15): ionic Pt in SSZ-13 is unstable at temperatures > 400 °C, even when O_2 is present in the gas-phase and thermal treatment leads to the formation of metallic Pt particles. FTIR spectra of adsorbed CO on the 400 °C-calcined 1 wt% Pt/SSZ-13 showed a prominent feature approximately 2090 cm^{-1}, confirming the formation of metallic Pt clusters (Figure S16).[11,50]

In summary, we provide a direct, simple, and scalable route to highly loaded ionic Pd and Pt in a small-pore siliceous (3 < Si/Al < 12) zeolite. This route utilizes only wet chemistry and does not require the use of expensive organometallic precursors or organic solvents. The key is to use the NH_4-form of the zeolite and the modified IWI method, not the conventional ion exchange. Furthermore, we reconcile the contradictory literature data which the FTIR characterization for high loaded Pt and Pd species in ZSM-5 and other zeolites

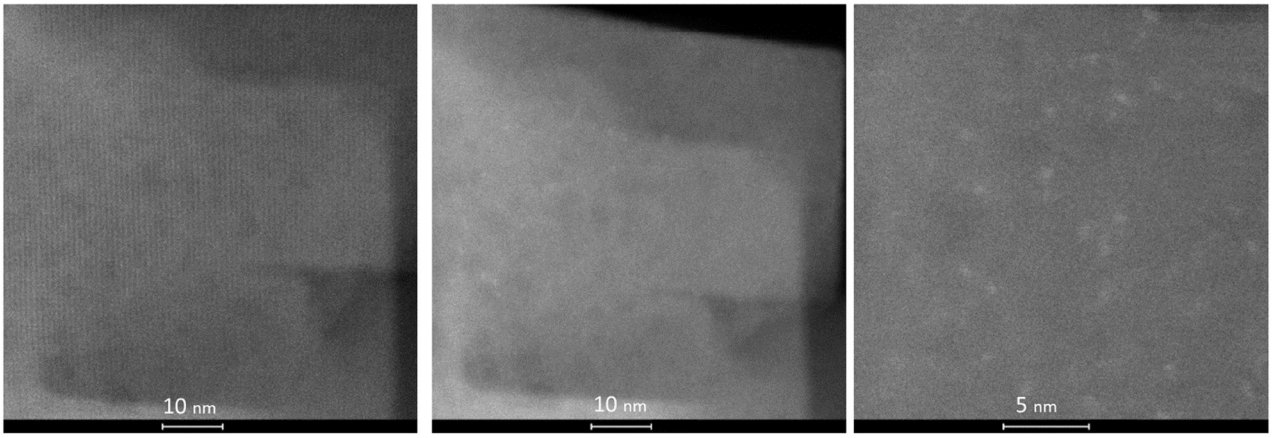

Figure 5. HAADF-STEM consecutive images (images takes in 20 sec time intervals) of 1 wt% Pt/H-SSZ-13 with Si/Al = 6; the images show the evolution during imaging: when we are able to catch the intact CHA framework, no Pt clusters are observed; however, under the beam within seconds the framework collapses and only during this collapse are Pt clusters formed. See Figure S12–S14 for other representative images of this sample.

always indicates the presence of significant amounts of metallic nanoparticles (not well-dispersed Pd or Pt) because: 1) H-forms of zeolite are often used for ion exchange, 2) Si/Al ratios > 10 are not able to disperse metals as individual atoms because of the decreased hydrophilicity of the zeolite micropores 3) For Pt, the calcination temperature should not exceed 350 °C because of the instability of ionic Pt^{2+} above this temperature. This new insight led to the synthesis of Pd/SSZ-13 with up to 2 wt% of atomically dispersed Pd for immediate industrial application as CO and passive NO_x adsorbers. These materials are able to abate 180 μmole g^{-1} NO_x and simultaneously CO during cold-start of the vehicle while maintaining atomic dispersion. We achieved complete utilization of each Pd atom, surpassing the best performance of Pd/zeolite adsorbers reported in both patent[38,39] and open[35–37,40–45] literature.

Acknowledgements

We gratefully acknowledge the U.S. Department of Energy (DOE),Office of Energy Efficiency and Renewable Energy, Vehicle Technologies Program for the support of this work. Most of the research described in this paper was performed in the Environmental Molecular Sciences Laboratory (EMSL), a national scientific user facility sponsored by the DOE's Office of Biological and Environmental Research and located at the Pacific Northwest National Laboratory (PNNL). PNNL is operated for the US DOE by Battelle. H.A.A. and I.Z.K. acknowledge financial support by the Bulgarian Science Fund (project DFNI-T02/20). H.A.A., G.N.V., and I.Z.K. acknowledge financial support by the European Regional Development Fund and the Operational Program "Science and Education for Smart Growth" under contract UNITe No. BG05M2OP001-1.001-0004-C01 (2018–2023). F.T., Y.T. and X.Z. acknowledge the support of their work by the Chemical Sciences, Geosciences and Biosciences Division, Office of Basic Energy Sciences, Office of Science, U.S. Department of Energy, under Grant No. DE-SC0014561 and National Science Foundation under the grant No. NSF-OIA-1539105. K.K. would like to dedicate this work to Professor John R. Monnier on occasion of his election to the National Academy of Engineering: with gratitude for your friendship!

Conflict of interest

K.K., J.Sz., L.K., N.R.J., F.G., Y.W. (all from PNNL) filed for a patent.

Keywords: CO adsorber · NO_x · palladium · platinum · zeolites

How to cite: *Angew. Chem. Int. Ed.* **2018**, *57*, 16672–16677
Angew. Chem. **2018**, *130*, 16914–16919

[1] W. M. H. Sachtler, *Catal. Today* **1992**, *15*, 419–429.
[2] "Noble Metal Alkaline Zeolites for Catalytic Reforming": A. E. Schweizer, US Patent 4992401, **1991**.
[3] K. Klier, *Langmuir* **1988**, *4*, 13–25.
[4] F. Lónyi, A. Kovács, A. Szegedi, J. Valyon, *J. Phys. Chem. C* **2009**, *113*, 10527–10540.
[5] A. Corma, H. García, *Top. Catal.* **2008**, *48*, 8–31.
[6] M. Haruta, *Chem. Rec.* **2003**, *3*, 75–87.
[7] M. R. Barrer, *Zeolite Synthesis: An Overview, Surface Organometallic Chemistry: Molecular Approaches to Surface Catalysis*, **1998**, *221–244*.
[8] J.-H. Kwak, D. Tran, S. D. Burton, J. Szanyi, J. H. Lee, C. H. F. Peden, *J. Catal.* **2012**, *287*, 203–209.
[9] B. Delmon, G. F. Froment, *Stud. Surf. Sci. Catal.* **1994**, *88*, 129–144.
[10] W. M. H. Sachtler, *Acc. Chem. Res.* **1993**, *26*, 383–387.
[11] K. Ding, A. Gulec, A. M. Johnson, N. M. Schweitzer, G. D. Stucky, L. D. Marks, P. C. Stair, *Science* **2015**, *350*, 189–192.
[12] M. Ranocchiari, J. A. Van Bokhoven, *Acc. Chem. Res.* **2017**, *50*, 418–425.
[13] J.-H. Kwak, J. Hu, D. Mei, C.-W. Yi, D. H. Kim, C. H. F. Peden, L. F. Allard, J. Szanyi, *Science* **2009**, *325*, 1670–1673.
[14] L. Liu, A. Corma, *Chem. Rev.* **2018**, *118*, 4981–5079.

[15] H. Yang, H. Chen, J. Chen, O. Omotoso, Z. Ring, *J. Catal.* **2006**, *243*, 36 – 42.
[16] M. Moliner, J. E. Gabay, C. E. Kliewer, R. T. Carr, J. Guzman, G. L. Casty, P. Serno, A. Corma, *J. Am. Chem. Soc.* **2016**, *138*, 15743 – 15750.
[17] D. Wang, W. Epling, I. Nova, J. Szanyi, *Catal. Today* **2016**, *267*, 1 – 2.
[18] "Zeolite SSZ-13 and its method of preparation": S. I. Zones, US patent 4544538, **1985**.
[19] J.-H. Kwak, R. G. Tonkyn, D. H. Kim, J. Szanyi, C. H. F. Peden, *J. Catal.* **2010**, *275*, 187 – 190.
[20] F. Gao, D. Mei, Y. Wang, J. Szanyi, C. H. F. Peden, *J. Am. Chem. Soc.* **2017**, *139*, 4935 – 4942.
[21] J. H. Kwak, J. H. Lee, S. D. Burton, A. S. Lipton, C. H. F. Peden, J. Szanyi, *Angew. Chem. Int. Ed.* **2013**, *52*, 9985 – 9989; *Angew. Chem.* **2013**, *125*, 10169 – 10173.
[22] V. L. Sushkevich, D. Palagin, J. A. Van Bokhoven, *Angew. Chem. Int. Ed.* **2018**, *57*, 8906 – 8910; *Angew. Chem.* **2018**, *130*, 9044 – 9048.
[23] F. Gao, J. Szanyi, *Appl. Catal. A* **2018**, *560*, 185 – 194.
[24] B. Zhan, E. Iglesia, *Angew. Chem. Int. Ed.* **2007**, *46*, 3697 – 3700; *Angew. Chem.* **2007**, *119*, 3771 – 3774.
[25] M. Choi, Z. Wu, E. Iglesia, *J. Am. Chem. Soc.* **2010**, *132*, 9129 – 9137.
[26] K. I. Hadjiivanov, G. N. Vayssilov, *Adv. Catal.* **2002**, *47*, 307 – 511.
[27] A. W. Aylor, L. J. Lobree, J. A. Reimer, A. T. Bell, *J. Catal.* **1997**, *172*, 453 – 462.
[28] K. Chakarova, E. Ivanova, K. Hadjiivanov, D. Klissurski, H. Knözinger, *Phys. Chem. Chem. Phys.* **2004**, *6*, 3702 – 3709.
[29] M. Rivallan, E. Seguin, S. Thomas, M. Lepage, N. Takagi, H. Hirata, T.-F. Starzyk, *Angew. Chem. Int. Ed.* **2010**, *49*, 785 – 789; *Angew. Chem.* **2010**, *122*, 797 – 801.
[30] K. Chakarova, M. Mihaylov, K. Hadjiivanov, *Microporous Mesoporous Mater.* **2005**, *81*, 305 – 312.
[31] K. Chakarova, M. Mihaylov, K. Hadjiivanov, *Catal. Commun.* **2005**, *6*, 466 – 471.
[32] W. Huang, S. Zhang, Y. Tang, Y. Li, L. Nguyen, Y. Li, J. Shan, D. Xiao, R. Gagne, A. I. Frenkel, F. Tao, *Angew. Chem. Int. Ed.* **2016**, *55*, 13441 – 13445; *Angew. Chem.* **2016**, *128*, 13639 – 13643.
[33] A. M. Beale, F. Gao, I. Lezcano-Gonzalez, C. H. F. Peden, J. Szanyi, *Chem. Soc. Rev.* **2015**, *44*, 7371 – 7405.
[34] S. Shwan, M. Skoglundh, L. F. Lundegaard, R. Tiruvalam, T. Janssens, A. Carlsson, P. N. R. Vennestrøm, *ACS Catal.* **2015**, *5*, 16 – 19.
[35] J. E. Melville, R. J. Brisley, O. Keane, P. R. Phillips, E. H. Mountstevens, US Patent US8105559B2, **2012**.
[36] J. A. Cole, US Patent US5656244A, **1997**.
[37] Y. Murata, T. Morita, K. Wada, H. Ohno, *SAE Int. J. Fuels Lubr.* **2015**, *8*, 454 – 459.
[38] R. R. Rajaram, H.-Y. Chen, D. Liu, US Patent US20150158019A1, **2015**.
[39] H.-Y. Chen, J. E. Collier, D. Liu, L. Mantarosie, D. Duran-Martin, V. Novak, R. Rajaram, D. Thompsett, *Catal. Lett.* **2016**, *146*, 1706 – 1711.
[40] Y. Ji, S. Bai, M. Crocker, *Appl. Catal. B* **2015**, *170 – 171*, 283 – 292.
[41] S. Jones, Y. Ji, M. Crocker, CeO_2-M_2O_3 Passive NO_x Adsorbers for Cold Start Applications, CLEERS Workshop, **2016**.
[42] Y. Zheng, L. Kovarik, M. H. Engelhard, Y. Wang, Y. Wang, F. Gao, J. Szanyi, *J. Phys. Chem. C* **2017**, *121*, 15793 – 15803.
[43] J. R. Theis, C. K. Lambert, *Catal. Today* **2017**, https://doi.org/10.1016/j.cattod.2017.12.014.
[44] A. Vu, J. Luo, J. Li, W. S. Epling, *Catal. Lett.* **2017**, *147*, 745 – 750.
[45] Y. Ryou, J. Lee, H. Lee, S. J. Cho, H. Lee, C. H. Kim, D. H. Kim, *Appl. Catal. B* **2017**, *215*, 140 – 149.
[46] K. Khivantsev, F. Gao, L. Kovarik, Y. Wang, J. Szanyi, *J. Phys. Chem. C* **2018**, *122*, 10820 – 10827.
[47] N. N. Greenwood, A. Earnshaw, *Chemistry of the Elements*, Pergamon, Oxford, **1984**, pp. 1336 – 1337. ISBN 0-08-022057-6.
[48] J. P. Collins, J. D. Way, *J. Membr. Sci.* **1994**, *96*, 259 – 274.
[49] Storing and handling ammonium nitrate, http://www.hse.gov.uk/pubns/indg230.pdf.
[50] H. A. Aleksandrov, K. M. Neyman, K. Hadjiivanov, G. N. Vayssilov, *Phys. Chem. Chem. Phys.* **2016**, *18*, 22108 – 22121.
[51] K. Hadjiivanov, J. Saussey, J. L. Freysz, J. C. Lavalley, *Catal. Lett.* **1998**, *52*, 103 – 108.
[52] J. Szanyi, M. T. Paffett, *J. Catal.* **1996**, *164*, 232 – 245.
[53] K. Khivantsev, A. Vityuk, H. A. Aleksandrov, G. N. Vayssilov, D. Blom, O. S. Alexeev, M. D. Amirdis, *ACS Catal.* **2017**, *7*, 5965 – 5982.
[54] T. W. Hayton, P. Legzdins, W. B. Sharp, *Chem. Rev.* **2002**, *102*, 935 – 991.

Manuscript received: August 19, 2018
Accepted manuscript online: October 16, 2018
Version of record online: November 12, 2018

